

Aquatic chemistry and solubility phenomena of actinide oxides/hydroxides*

Th. Fanghänel[‡] and V. Neck

*Forschungszentrum Karlsruhe, Institut für Nukleare Entsorgung, Postfach 3640,
D-76021 Karlsruhe, Germany*

Abstract: The present paper gives an overview of the solubility behavior of actinide oxides/hydroxides, taking into account hydrolysis reactions up to colloid formation. The analogies, systematic trends, and differences in the hydrolysis and solubility constants of actinides in the oxidation states An(III) to An(VI) correlate with the charge and size of the actinide ions. The formation of amorphous and crystalline solids and the discrepancies between the corresponding experimental solubility data may be explained as an effect of particle size. However, using thermodynamic data for the stable crystalline solids, the predicted solubilities are often significantly lower than experimental data (even in long-time experiments), indicating that the solubility is controlled by the surface properties. Typical examples are the known U(VI) solids schoepite and sodium diuranate. The most striking example is provided by the tetravalent actinides. Above the threshold of hydrolysis, the dissolution of microcrystalline or crystalline An(IV) oxides is found to be irreversible. The measured concentrations approach those of the amorphous hydroxides or hydrous oxides.

INTRODUCTION

The solubility and aqueous speciation of actinides is of particular interest for their geochemical modeling in natural aquatic systems with regard to the safety of nuclear waste disposal. Among numerous reactions that govern the chemical behavior of trace actinides, the knowledge of hydrolysis and carbonate complexation is of highest priority. Depending on the site-specific geochemical conditions, the complexation with other inorganic ligands (such as chloride, sulfate, phosphate, fluoride, silicate) or organic substances may become important as well. In simple laboratory systems, the concentration of actinides in aqueous solutions is primarily limited to the solubility of their hydroxides, oxides, and carbonate solid phases. In some cases, the solubility is limited by ternary solids with mono- or divalent metal ions like Na⁺. The solubilities determined in laboratory experiments can be considered as the conservative upper limit for actinide concentrations. In real systems, the trace concentration of actinides can be decreased by sorption on the geomatrix, coprecipitation, and formation of solid solutions.

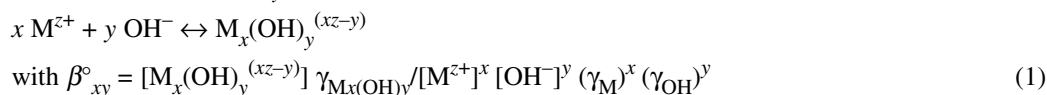
The present paper is restricted to the discussion of the solubility of oxides and hydroxides and the hydrolysis reactions. The thermodynamic data discussed are primarily taken from the hitherto published NEA-TDB reviews [1–3], taking into account new selections or changed values from the ongoing NEA-TDB project (phase II) [4], which is aimed at the update of the chemical thermodynamics of U, Np, Pu, Am, and Tc.

*Lecture presented at the 10th International Symposium on Solubility Phenomena, Varna, Bulgaria, 22–26 July 2002. Other lectures are published in this issue, pp. 1785–1920.

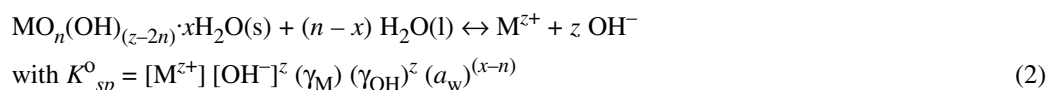
[‡]Corresponding author

DEFINITIONS AND TERMINOLOGY

Throughout the present paper, the hydrolysis reactions of a metal ion M^{z+} is written as the formation of hydroxide complexes $M_x(OH)_y^{(xz-y)}$ according to



where β_{xy}° is the equilibrium constant at $I = 0$, and γ_i is the activity coefficient of species i . M stands for An^{3+} and An^{4+} in the case of tri- and tetravalent actinides or AnO_2^+ and AnO_2^{2+} in the case of penta- and hexavalent actinides. The solubility products of hydroxides and oxides (K_{sp}° at $I = 0$ and K'_{sp} in a given medium) are defined according to the dissolution equilibrium



For the conversion of conditional constants, i.e., concentration products/quotients β'_{xy} and K'_{sp} in a given medium, into equilibrium constants at $I = 0$, activity coefficients are calculated with the ion interaction (SIT) coefficients recommended in the NEA-TDB [1–4]. If there are no other complexes or colloidal species present in solution, the total metal concentration is given by

$$[M]_{\text{tot}} = [M^{z+}] + \sum x [M_x(OH)_y^{(xz-y)}] = K'_{sp} [OH^-]^{-n} + \sum x \{ (K'_{sp} [OH^-]^{-n})^x \beta'_{xy} [OH^-]^y \} \quad (3)$$

OXIDATION STATE ANALOGIES AND SYSTEMATIC TRENDS

It is well known that there are pronounced similarities and analogies in most chemical properties of the actinide elements in the oxidation states An(III, IV, V or VI), with the exception of their redox properties [5,6]. Certain systematic trends in the thermodynamic data and equilibrium constants often correlate with the variation of the effective charge and ionic radius. This chemically well-established principle can be used to compare and estimate three different types of thermodynamic data:

- activity coefficients/ion interaction parameters of aqueous species
- formation constants of aqueous complexes
- solubility constants of isostructural solids

Due to specific experimental difficulties or due to the lack of appropriate experimental and analytical methods at trace concentration levels, a number of thermodynamic data cannot be determined experimentally. For instance, equilibrium constants determined by time-resolved laser fluorescence spectroscopy (TRLFS) at Cm(III) concentrations $\leq 10^{-7}$ mol/l [7] are often more accurate than those determined with experimental methods applicable to Am(III). For reasons of easier handling, the non-radioactive lanthanides Nd(III) and Eu(III) are also often studied as analogs for Am(III). In the case of penta- and hexavalent actinides, the chemical thermodynamics of Np(V) and U(VI) are well investigated, whereas the information on Pu(V) and Am(V) or Np(VI) and Pu(VI) is rather poor, because the determination of thermodynamic data for actinides in less-stable oxidation states is usually complicated by the interference of redox reactions. In such cases, it is helpful to use data from well-ascertained oxidation state analogs as reasonable estimates.

Activity coefficients

The activity coefficient of an aqueous species depends on its interactions with the ions in solution and H_2O solvent molecules. In general, small differences in the size of aquo ions or complexes of equal charge and symmetry have only a slight effect on the activity coefficients. Ion interaction coefficients

can be set equal for aquo ions and analogous complexes of Nd^{3+} and An^{3+} (for $\text{An} = \text{Pu}, \text{Am}, \text{Cm}$), AnO_2^+ (for $\text{An} = \text{U}, \text{Np}, \text{Pu}, \text{Am}$), and AnO_2^{2+} (for $\text{An} = \text{U}, \text{Np}, \text{Pu}$) [1–4,7,8]. In the case of the An^{4+} aquo ions ($\text{An} = \text{Th}, \text{U}, \text{Np}, \text{Pu}$), the high charge and the larger differences in ionic radii lead to certain differences in the activity coefficients [3,4,9].

Hydrolysis and complexation constants

Hydrolysis and complexation constants of metal ions are known to correlate with the electrostatic interaction energy between the metal and ligand ions [5,6,10,11]:

$$\log \beta_{(M)}^{\circ} \propto {}^{\text{el}}E_{\text{M-L}} \propto (z_{\text{M}}/d_{\text{M-L}}) \quad (4)$$

where z_{M} is the charge of the metal ion and $d_{\text{M-L}}$ the distance between the centers of metal and ligand ions. This empirical linear correlation led to effective charges of $z_{\text{M}} = 2.3 \pm 0.1$ and 3.2 ± 0.1 for the penta- and hexavalent actinide ions AnO_2^+ and AnO_2^{2+} , respectively [5,6]. Figure 1a shows the application of correlation (4) to the known hydrolysis constants of Am^{3+} and Cm^{3+} , An^{4+} ($\text{An} = \text{Th}, \text{U}, \text{Np}, \text{Pu}$), NpO_2^+ , and UO_2^{2+} .

Considering the similar ionic radii of Am^{3+} and Cm^{3+} (110 and 109 pm, respectively [6,12]), it is not surprising that the real differences between the formation constants of Am(III) and Cm(III) complexes are smaller than the experimental uncertainties [13]. Formation constants of analogous hydroxide and carbonate complexes of Np(V) and Am(V) were also found to be equal within the range of experimental errors [14,15]. However, in the case of the somewhat smaller AnO_2^{2+} ions, the oxidation state analogy is more restricted. For sterical reasons, the formation constants of the bidentate carbonate complexes, in particular $\log \beta_2$ and $\log \beta_3$ [8], and of polynuclear An(VI) hydrolysis species [16] decrease in the series $\text{U(VI)} > \text{Np(VI)} > \text{Pu(VI)}$. In the series of the tetravalent actinides, the distance $d_{\text{An-OH}}$ decreases more distinctly (from 246 to 242, 240, and 239 pm [17]) and accordingly, the complex formation constants increase considerably in the series $\text{Th(IV)} < \text{U(IV)} < \text{Np(IV)} < \text{Pu(IV)}$. The large differences between the hydrolysis constants $\log \beta_{1n}^{\circ}$ of Th^{4+} compared to those of other An^{4+} ions arise not only from differences in the ionic size, but also from differences in the electronic configuration.

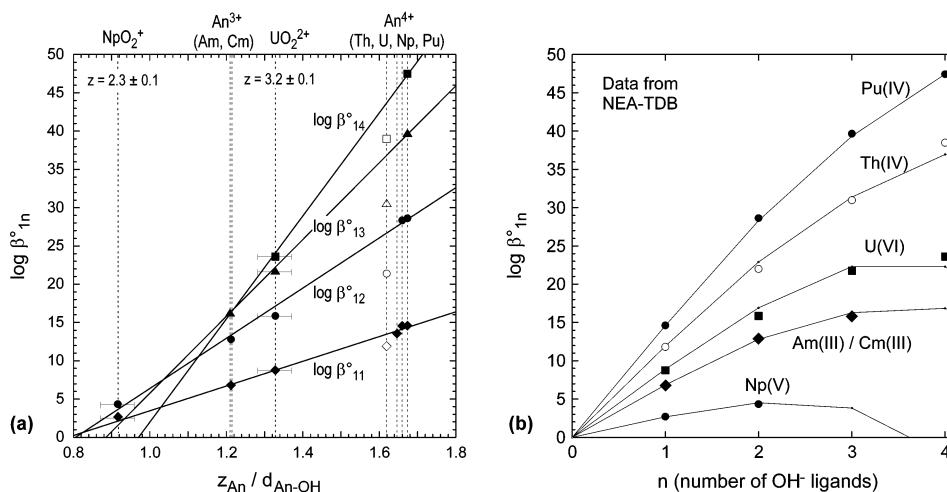


Fig. 1 Formation constants of mononuclear actinide hydroxide complexes. (a) Correlation between $\log \beta_{1n}^{\circ}$ and the electrostatic interaction energy between the actinide and OH^- ions; z_{An} = effective charge, $d_{\text{An-OH}}$ = distance (taken from the compilation in [17]). (b) Application of the ligand repulsion approach of Neck and Kim [17] (solid lines) to describe $\log \beta_{1n}^{\circ}$ as a function of n , the number of OH^- ligands.

The systematic decrease of stepwise complexation constants can be described by an electrostatic approach [17]. The mononuclear formation constants $\log \beta_n^\circ$ for a given actinide ion are related with an inter-ligand Coulomb repulsion term ${}^{\text{rep}}E_L$, which increases with n , the number of ligands:

$$\log \beta_n^\circ = n \log \beta_1^\circ - {}^{\text{rep}}E_L/RT \ln 10 \quad (5)$$

The application of eq. 5, with the parameters for OH^- ligands taken from [9], is shown in Fig. 1b. Because of the high charge density of actinide ions, which is decreasing in the series $\text{An}^{4+} > \text{AnO}_2^{2+} > \text{An}^{3+} > \text{AnO}_2^+$, the initial hydrolysis starts in acidic to neutral solutions, in the case of AnO_2^+ in the alkaline range. In addition, the hexa- and tetravalent actinides are known to undergo polynucleation reactions, up to the formation of colloidal species.

Solid phases and solubility constants

Actinides (and also lanthanides) of the same oxidation state and similar size form oxide, hydroxide, and carbonate solid phases of analogous stoichiometries and crystal structures. However, small differences in the radii of the metal ions can cause significant differences in the lattice energy and hence in the solubility products. The solubility products of the amorphous An(IV) hydroxides and the isostructural dioxides $\text{AnO}_2(\text{cr})$ decrease orders of magnitude in the series $\text{Th(IV)} > \text{U(IV)} > \text{Np(IV)} > \text{Pu(IV)}$ (c.f. Table 1), which correlates with the decreasing distance $d_{\text{An-O}}$ in the lattice [12]. The differences in $\log K_{\text{sp}}^\circ$ of An(VI) hydroxides and carbonates are relatively small, and the solubility of Am(V) and Np(V) hydroxides $\text{AnO}_2(\text{OH})(\text{am})$ and carbonates $\text{NaAnO}_2\text{CO}_3 \cdot x\text{H}_2\text{O}(\text{s})$ were found to be identical [14,15]. Obviously, the solubility products of actinyl-ion salts are not significantly affected by the small differences in the central An(V) or An(VI) ions.

Table 1 Solubility products $\log K_{\text{sp}}^\circ$ of actinide oxides/hydroxides at 25 °C (from the NEA-TDB reviews [1–4] and values for $\text{An}(\text{OH})_4(\text{am})$ from ref. [9], except otherwise stated).

	Th	U	Np	Pu	Am
$\text{AnO}_2\text{OH}(\text{am})$			-8.7 ± 0.2	-9.0 ± 0.5	-8.7 ± 0.5
$\text{AnO}_2(\text{OH})_2(\text{s})$		$-22.8 \pm 0.4^{\text{a}}$	-22.5 ± 0.4	-22.5 ± 1.0	
$\text{AnO}_3 \cdot 2\text{H}_2\text{O}(\text{cr})$		$-23.2 \pm 0.4^*$			
$\text{An}(\text{OH})_3(\text{am})$				-26.2 ± 1.5	-25.1 ± 0.8
$\text{An}(\text{OH})_3(\text{cr})$					-26.4 ± 0.6
$\text{An}(\text{OH})_4(\text{am})$	-47.0 ± 0.8	-54.5 ± 1.0	-56.7 ± 0.5	-58.5 ± 0.7	
$\text{AnO}_2(\text{cr})$	$-53.2 \pm 0.4^{\text{b}}$				
	$-54.2 \pm 1.3^{\text{c}}$	$-60.9 \pm 0.4^*$	$-63.7 \pm 1.8^{\text{c}}$	$-64.0 \pm 0.5^*$	$-65.4 \pm 1.7^*$

*Calculated from thermochemical data.

^aMean value from solubility studies [26–31] discussed in ref. [4].

^bFrom solubility data for microcrystalline thorium dioxide [50].

^cFrom Rai et al. [18]. A noticeable deviation is observed for the NEA-TDB value of $\log K_{\text{sp}}^\circ[\text{NpO}_2(\text{cr})] = -65.8 \pm 1.1$ calculated with $S_{\text{m}}^\circ[\text{Np}^{4+}(\text{aq})] = -(426 \pm 12) \text{ JK}^{-1}\text{mol}^{-1}$ [3], which differs from $S_{\text{m}}^\circ[\text{Np}^{4+}(\text{aq})] = -(389 \pm 21) \text{ JK}^{-1}\text{mol}^{-1}$ [19] used by Rai et al. [18].

SOLUBILITY PHENOMENA

The molar standard Gibbs energies of formation $\Delta_{\text{f}}G_{\text{m}}^\circ$ and, hence, the solubility products of numerous solid phases can be derived from thermochemical data based on calorimetric measurements with well-defined and well-characterized dried solids. They are calculated from the standard enthalpies of forma-

tion $\Delta_r H_m^\circ$, derived from the experimental values for the enthalpy of dissolution, combined with the standard entropies S_m° , and auxiliary data for the actinide aqueous ions, H^+ , OH^- , and $H_2O(l)$. On the contrary, the solubility constants determined from solubility experiments usually refer to solid phases formed by precipitation and subsequent alteration. Equilibrium constants for the dissolution of actinide oxides and hydroxides are partly ascribed to amorphous, partly to crystalline solids, usually according to the characterization by XRD. However, the appearance of XRD peaks does not exclude the fact that large parts of the solid or the surface are still amorphous. Particularly amorphous solids are often not very well chemically defined. Their standard molar Gibbs energy depends on particle size, hydrated surface area, and content of crystal water, which are in most cases not exactly known.

For kinetics reasons, metastable solid phases or solids consisting of agglomerates of small particles (<100 nm) are frequently observed as the solubility-limiting solid phase. Even in the case of initially crystalline solids, a less-crystalline solid or an amorphous surface layer can be formed by α -radiation damage or by dissolution-precipitation reactions, respectively. Therefore, solubilities calculated from thermodynamic data of the well-crystallized (thermodynamically stable) solids are often considerably lower than those derived from experimental solubility data. In the following sections, the solubility behavior of actinide hydroxides and oxides is discussed in the order of the nominal charge of the actinide aquo ions AnO_2^+ , AnO_2^{2+} , An^{3+} , and An^{4+} using experimental data for redox-stable surrogates in the corresponding oxidation state.

Fresh and aged Np(V) hydroxide

The solubility of amorphous Np(V) hydroxide, $NpO_2OH \cdot xH_2O(am)$, is well ascertained by experimental studies [14,20–22] in solutions with a wide variety of ionic strength. The crystal water content was determined to be $x = 2.5$ [23]. Neck et al. [21] and Runde [14] observed the aging or ripening of the fresh amorphous precipitate in 1 and 3 M $NaClO_4$ and in 5 M $NaCl$, respectively (c.f. Fig. 2). The solubility of the aged Np(V) hydroxide decreased about 0.6 log-units $\{\log K_{sp}^\circ(NpO_2OH, \text{aged}) = -9.3 \pm 0.5$ compared to $\log K_{sp}^\circ(NpO_2OH, \text{am, fresh}) = -8.7 \pm 0.2$ [3]}. Unfortunately, the aged solid was not characterized by XRD. Its solubility product is still significantly higher than the thermochemical value of $\log K_{sp}^\circ = -12.2 \pm 0.8$ calculated from NEA-TDB data for the thermodynamically stable oxide

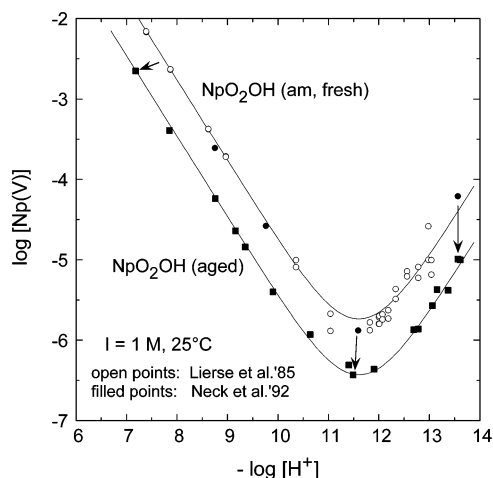


Fig. 2. Solubility of fresh and aged precipitates of amorphous Np(V) hydroxide at 25 °C in 1 M $NaClO_4$ – $NaOH$ [20,21]. The corresponding equilibrium constants selected in the NEA-TDB are $\log K_{sp}^\circ = -8.7 \pm 0.2$ and -9.3 ± 0.5 , respectively, $\log \beta_{11}^\circ = 2.7 \pm 0.7$ and $\log \beta_{12}^\circ = 4.4 \pm 0.5$ [3].

$\text{Np}_2\text{O}_5(\text{cr})$ or the values of -10.1 ± 0.2 [24] and -11.4 ± 0.4 [25] determined in solubility studies with hydrated $\text{Np}_2\text{O}_5(\text{s})$.

U(VI) oxides/hydroxides: solubility measurements and thermochemical data

The solubility-limiting U(VI) oxide/hydroxide phases in sodium salt solutions are known to be schoepite and sodium uranates of various crystallinity. The composition of the thermodynamically stable phase depends on the composition of the ionic medium, in particular on the Na^+ and OH^- concentrations. (It is difficult to distinguish whether these solids are hydrated oxides, hydroxides, or oxyhydroxides. The structure of the uranyl ion is retained in these solids, which is more clearly represented by the formulation as hydroxides.) The thermochemical data for well-crystallized $\text{UO}_3 \cdot 2\text{H}_2\text{O}(\text{cr})$ and $\text{Na}_2\text{U}_2\text{O}_7(\text{cr})$ lead to $\log K_{\text{sp}}^\circ = -23.2 \pm 0.4$ and -30.7 ± 0.5 , respectively [1]. These calculated solubility products are about 0.5–1 log-units lower than those determined from solubility data. Numerous solubility studies [26–31] performed with more or less crystalline $\text{UO}_3 \cdot 2\text{H}_2\text{O}(\text{s, hydr})$ or $\text{UO}_2(\text{OH})_2(\text{s})$ yield an average value of $\log K_{\text{sp}}^\circ = -22.8 \pm 0.4$ [4], and a solubility study with $\text{Na}_2\text{U}_2\text{O}_7(\text{s, hydr})$ or $\text{NaUO}_2(\text{OH})_3(\text{s})$ led to $\log K_{\text{sp}}^\circ = -29.45 \pm 1.04$ [32].

In a recent study from our laboratory [33], these experimental solubility products have been confirmed (Fig. 3). Adding microcrystalline $\text{UO}_2(\text{OH})_2(\text{s})$ to a solution of pH 10 in 0.5 M NaCl, the pH decreased to a value of 8 according to the dissolution reaction



and a steady-state U(VI) concentration was reached, which remained constant up to 60 days. After 80–120 days, the U(VI) concentration decreased due to the precipitation of $\text{NaUO}_2(\text{OH})_3(\text{s})$ as expected according to the thermodynamic stability of these solids. In an analogous experiment in 5 M NaCl, the transformation of $\text{UO}_2(\text{OH})_2(\text{s})$ into $\text{NaUO}_2(\text{OH})_3(\text{s})$ started immediately and was completed after 80 days. The solid formed was identified by XRD analysis as Clarkeite $\text{NaUO}_2\text{O}(\text{OH}) \cdot \text{H}_2\text{O}(\text{cr})$ [chemical composition equal to $\text{NaUO}_2(\text{OH})_3(\text{s})$ or $1/2 \text{Na}_2\text{U}_2\text{O}_7 \cdot 3\text{H}_2\text{O}(\text{cr})$]. Using the hydrolysis constants of the NEA-TDB [4] as fixed values, the solubility data determined for $\text{UO}_2(\text{OH})_2(\text{s})$ yield $\log K_{\text{sp}}^\circ = -22.6$ [33] and those measured after solid transformation are consistent with $\log K_{\text{sp}}^\circ = -29.45 \pm 1.04$ for $\text{Na}_2\text{U}_2\text{O}_7(\text{s, hydr})$ [32].

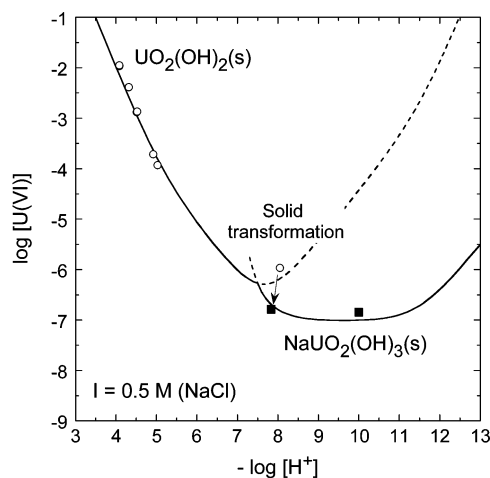


Fig. 3. Solubility of U(VI) at 25 °C in 0.5 M NaCl and the transformation of $\text{UO}_2(\text{OH})_2(\text{s})$ into $\text{NaUO}_2(\text{OH})_3(\text{s})$ [33]. The calculated lines are based on the hydrolysis constants selected by the NEA-TDB [1,4], $\log K_{\text{sp}}^\circ[\text{UO}_2(\text{OH})_2(\text{s})] = -22.6$ [33] and $\log K_{\text{sp}}^\circ[\text{NaUO}_2(\text{OH})_3(\text{s})] = -29.45$ [32].

Amorphous and crystalline Am(III) hydroxide

The thermodynamic properties and hence the solubility of $\text{Am}(\text{OH})_3(\text{s})$ depends on the degree of crystallinity, which is affected by aging or ripening processes and by self-irradiation from the α -activity of americium, particularly in studies with ^{241}Am ($t_{1/2} = 433$ a). Experimental solubilities of americium(III) hydroxides are shown in Fig. 4. Silva's study [34] is the only one performed with a crystalline $\text{Am}(\text{OH})_3(\text{cr})$ characterized by XRD. The damage by α -radiation was diminished by the use of ^{243}Am ($t_{1/2} = 7370$ a). Concordant solubilities were measured by Stadler and Kim [35] at rather high specific α -activities of ^{241}Am . Rai et al. [36] determined the solubility of X-ray amorphous precipitates in dilute solutions containing $1.5 \cdot 10^{-3}$ M CaCl_2 . Comparable solubility data for $\text{Am}(\text{OH})_3(\text{am})$ were determined by Edelstein et al. [37,38] in 0.1 M NaClO_4 .

The use of the notation "crystalline" and "amorphous" to describe a solid phase and, thereby, its solubility might be an oversimplification. The XRD data give information of the bulk structure, while the solubility is determined by the surface characteristics. These are not necessarily identical. Nevertheless, the solubility products of $\log K_{\text{sp}}^\circ = -26.4 \pm 0.6$ and -25.1 ± 0.8 for "crystalline" and "amorphous" $\text{Am}(\text{OH})_3(\text{s})$, respectively, may indicate the magnitude of the effect of varying surface state of the solid. The value of $\Delta_f G_m^\circ[\text{Am}_2\text{O}_3(\text{cr})] = -(1613.3 \pm 9.2)$ kJ/mol [2] implies that Am(III) oxide is highly soluble and not stable in aqueous solution.

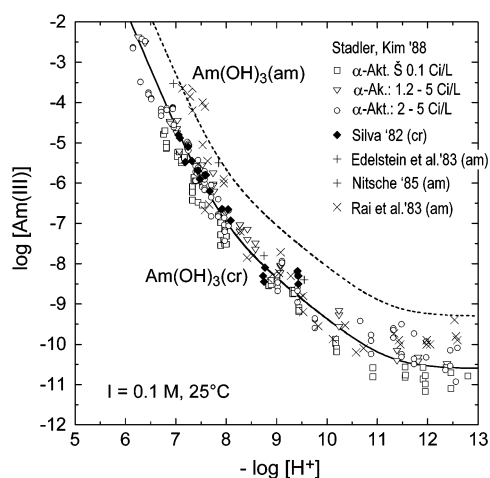


Fig. 4 Solubility of amorphous and crystalline Am(III) hydroxide at 25 °C and $I = 0.1$ M [34,35,37,38] and in dilute solutions [36]. The solid and dashed lines are calculated with $\log K_{\text{sp}}^\circ = -26.4 \pm 0.6$ and -25.1 ± 0.8 , respectively, $\log \beta_{11}^\circ = 6.8 \pm 0.5$, $\log \beta_{12}^\circ = 12.9 \pm 0.7$, and $\log \beta_{13}^\circ = 15.8 \pm 0.5$ [4].

Amorphous Th(IV) hydroxide: solubility increase caused by colloids

The solubility data determined with X-ray amorphous Th(IV) precipitates at $I = 0.1$ – 0.6 M (NaClO_4 , NaCl , or KCl media) and 17–25 °C are widely scattered (c.f. Fig. 5). Numerous studies were performed with fresh precipitates only washed with water [39–44]. Using a precipitate dried at room temperature, Östhols et al. [45] and Neck et al. [46] measured the solubility at 25 °C in 0.5 M NaClO_4 and NaCl , respectively. Their results at pH 3–5 are 3–4 orders of magnitude lower than those in [39–44], but still about 6 orders of magnitude higher than for crystalline $\text{ThO}_2(\text{cr})$.

A possible explanation for these discrepancies would be that the experimental data do not refer to a well-defined unique solid, but to hydrated oxyhydroxides $\text{ThO}_n(\text{OH})_{4-2n}(\text{am})$ with $0 < n < 2$, depending on the preparation method, pretreatment, and alteration. However, Neck et al. [46] clearly

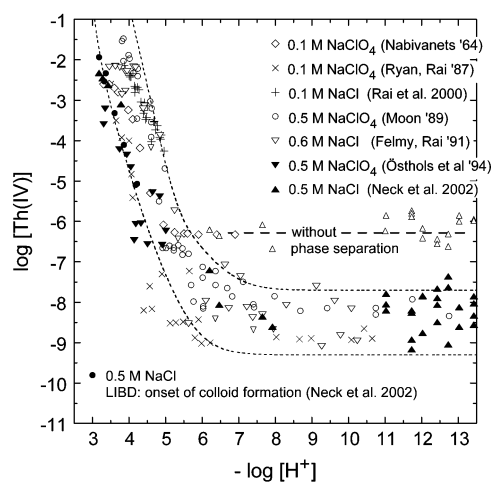


Fig. 5 Solubility of X-ray amorphous Th(IV) precipitates at 17–25 °C and $I = 0.1\text{--}0.6$ M (exp. data from [39–46]). The lower and upper dashed curves correspond to $\log K_{sp}^{\circ} = -47.8$ and -46.2 , respectively. The region between these curves is dominated by colloid formation. The calculated lines are based on hydrolysis constants $\log \beta_{1n}^{\circ} = 11.8, 22.0, 31.0, 38.5$ (for $n = 1\text{--}4$), and $\log \beta_{4,12}^{\circ} = 141.3$ [9,46].

demonstrated that the large discrepancies in the measured thorium concentrations are primarily caused by contributions from colloids. In this recent study, the laser-induced breakdown detection (LIBD) was applied to detect colloids of small size, and extended X-ray absorption fine structure (EXAFS) spectroscopy was used for the aqueous speciation up to pH 4. Coulometric pH titration was combined with the LIBD to monitor the initial colloid formation. Considering colloids as small solid particles, their formation indicates that the solubility is just exceeded during the titration. Hence, the H^{+} and Th(IV) concentrations at the onset of colloid formation, which were found to be consistent with the classical solubility data for the dried solid [45,46], define the solubility of $Th(OH)_4(am)$ excluding colloidal thorium species. The colloids formed at pH 3–5 (i.e., in suspensions between the lower and upper curve in Fig. 5) did neither redissolve nor precipitate. LIBD and ultrafiltration studies after 100–400 days showed that neither the colloidal thorium concentration nor the mean particle size changed noticeably, indicating that they might be stable or at least long-time metastable species [47]. Moreover, pH changes measured as a function of time indicated that freshly prepared Th(IV) hydroxide suspensions approach a steady state, where Th(IV) colloids are in equilibrium with ionic species [47].

The large scatter of experimental solubility data in alkaline solutions is probably due to the varying success in removal of colloids by filtration or centrifugation. Considerably higher but less-scattered thorium concentrations were measured in aliquots taken without phase separation: $\log [Th]_{tot} = -6.2 \pm 0.5$ [46]. The quantification and modeling of the total solubility of oxides/hydroxides increased by stable or metastable eigencolloids of highly charged actinide ions requires further experimental investigation. This is also of particular interest for oxides/hydroxide colloids of Fe, Al, and Si, because trace actinides may be sorbed onto or incorporated into these colloids and thus mobilized as pseudo-colloids.

Th(IV) oxide/hydroxide: solubility product and particle size effect

According to the equations of Schindler [48], the solubility product of oxide and hydroxide particles <300 nm depends noticeably on the particle size, because of the difference in Gibbs energy when either small solid particles or large crystals with negligible molar surface are suspended in water. For approx-

imately spherical ThO_2 particles with diameter d , the difference between the solubility product of small ThO_2 particles and $\log K_{\text{sp}}^\circ = -54.2 \pm 1.3$ for a large crystal of $\text{ThO}_2(\text{cr})$ is given by [49]:

$$\log K_{\text{sp}}^\circ(\text{particle size } d) = -54.2 + 23/d(\text{nm}) \quad (6)$$

Titration-LIBD experiments at $\text{pH} = 1.5\text{--}2.5$ led to the formation of small thorium dioxide colloids (16–23 nm) with a solubility product of $\log K_{\text{sp}}^\circ = -52.9 \pm 0.5$ [49], which is in excellent agreement with $d = 13\text{--}29$ nm as calculated with eq. 6. The solubility product determined after agglomeration and precipitation of microcrystalline $\text{ThO}_2 \cdot x\text{H}_2\text{O}(\text{mcr})$, $\log K_{\text{sp}}^\circ = -53.2 \pm 0.4$ [50], would correspond to a particle size of 16–58 nm. Transmission electron microscopy investigations on X-ray amorphous Th(IV) precipitates dried at room temperature ($\log K_{\text{sp}}^\circ = -47.8 \pm 0.3$ [46]) indicate the inclusion of small $\text{ThO}_2(\text{cr})$ crystallites in the range of 3–8 nm [51]. Accordingly, the experimental solubility data for Th(IV) oxides/hydroxides could indeed be ascribed to $\text{ThO}_2(\text{cr})$ as the only solid phase with the differences in $\log K_{\text{sp}}^\circ$ arising from the particle size effect (Fig. 6). However, such small particles have a large hydrated surface, with OH-groups determining the chemical properties. The large gap of more than 5 orders of magnitude between the solubility products determined for microcrystalline thorium dioxide particles and X-ray amorphous solids also suggests to distinguish between the thermodynamic data for crystalline $\text{ThO}_2(\text{cr})$ and amorphous solids $\text{ThO}_n(\text{OH})_{4-2n}x\text{H}_2\text{O}(\text{am})$, which may be called “ $\text{Th}(\text{OH})_4(\text{am})$ ”, “ $\text{ThO}_2x\text{H}_2\text{O}(\text{am})$ ” or “ $\text{ThO}_2(\text{am}, \text{hyd})$ ”.

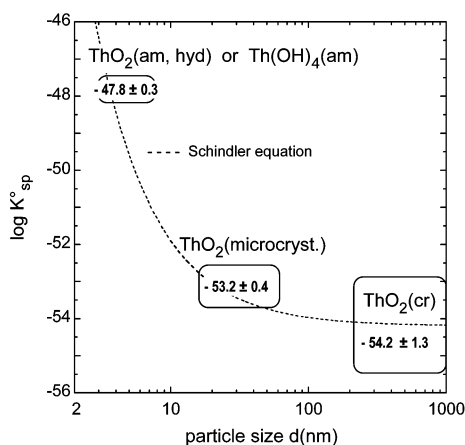


Fig. 6 Effect of particles size on the solubility products of crystalline, microcrystalline, and amorphous Th(IV) oxides/hydroxides ($I = 0$, 25°C). The dashed line is calculated by applying eq. 6 to $\text{ThO}_2(\text{cr})$.

Irreversible dissolution of crystalline An(IV) dioxides

Solubility experiments with well-crystallized $\text{ThO}_2(\text{cr})$ are related to the problem of very slow dissolution kinetics. Dissolution experiments in acidic solutions from undersaturation direction did not reach equilibrium after a period of one year [50,52], whereas equilibrium between $\text{Th}^{4+}(\text{aq})$ and microcrystalline thorium dioxide particles precipitated in the pH range of 1.5–2.5 could be achieved from oversaturation direction [50].

Contrary to the observations in these acidic solutions, the experimental solubility data determined with $\text{ThO}_2(\text{cr})$ [40,50] or microcrystalline $\text{ThO}_2 \cdot x\text{H}_2\text{O}(\text{mcr})$ [50] at $\text{pH} > 2.5$ exceed the solubility calculated for $\text{ThO}_2(\text{cr})$ after a few days (Fig. 7). In near-neutral and alkaline solutions, where $\text{Th}(\text{OH})_4(\text{aq})$ is the predominant complex and the solubility is independent of pH, the experimental data exceed the thermodynamic calculation by about 6 orders of magnitude and approach the values for

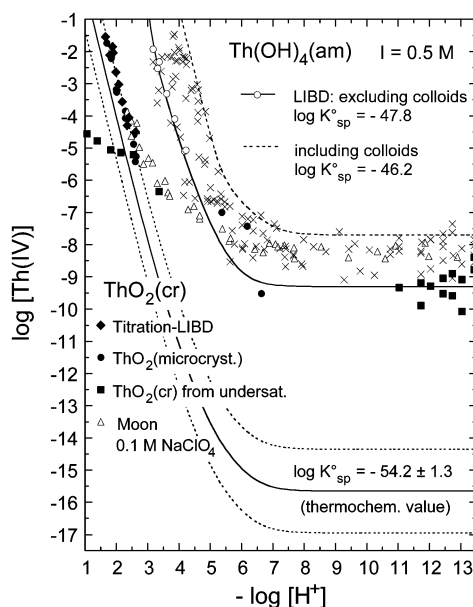
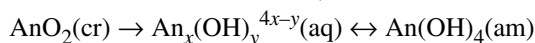


Fig. 7 Experimental and calculated solubility of $\text{ThO}_2(\text{cr})$ and $\text{Th}(\text{OH})_4(\text{am})$. The solubility data for $\text{ThO}_2(\text{cr})$ are determined in ref. [50] from undersaturation (filled squares) and oversaturation direction (filled circles) and by titration-LIBD (filled rhombs) in 0.5 M NaCl at 25 °C and from Moon [40] in 0.1 M NaClO_4 at 18 °C (open triangles). The solubility data for amorphous precipitates (x), at $I = 0.5\text{--}0.6$ M and 18–25 °C, are taken from refs. [40,42,43,45,46]. The lines are calculated for $I = 0.5$ M with the solubility products and hydrolysis constants discussed in refs. [9,46].

amorphous precipitates [40,50,52,53]. Solid–liquid equilibrium between thorium dioxide and aqueous Th(IV) species is observed only at $\text{pH} < 2.5$, where the Th^{4+} aquo ion is the predominant aqueous specie.

Similar observations in solubility studies with $\text{UO}_2(\text{cr})$ and $\text{PuO}_2(\text{cr})$ have been pointed out in ref. [9]. These experimental findings may simply be caused by the dissolution of small amounts of amorphous parts present in the crystalline solid, which remain dissolved as hydrolyzed species $\text{An}_x(\text{OH})_y^{4x-y}(\text{aq})$, suggesting that above the onset of hydrolysis, there is no reversible equilibrium between $\text{AnO}_2(\text{cr})$ and An(IV) hydrolysis species. The sorption or precipitation of monomeric or polynuclear hydroxide complexes $\text{An}_x(\text{OH})_y^{4x-y}(\text{aq})$ on the surface of crystalline $\text{AnO}_2(\text{cr})$ would lead to an amorphous surface layer. The slow dissolution of $\text{AnO}_2(\text{cr})$ followed by the very fast hydrolysis reactions of the An^{4+} ions might result in an irreversible dissolution reaction until the concentration of the hydroxide complexes $\text{An}_x(\text{OH})_y^{4x-y}(\text{aq})$ reach the solubility limit of “ $\text{An}(\text{OH})_4(\text{am})$ ”:



Comparing the impact of this effect on the solubility of oxides/hydroxides in the series of the tetravalent actinides (Fig. 8), it is noteworthy that the hydrolysis of the Th^{4+} ion starts at $\text{pH} 2.5\text{--}3$, about one pH-unit lower for U^{4+} and already at $\text{pH} 0\text{--}1$ for Np^{4+} and Pu^{4+} [4,9].

As a consequence of the experimental observations discussed in the present paper, conservative performance assessment model calculations should be based on thermodynamic data for solid phases actually observed as solubility-limiting solid in aqueous solution, i.e., on equilibrium constants from solubility studies. Thermodynamic data derived from calorimetric measurements with well-prepared, dried, ideally crystalline solids or high-temperature phases that are not formed in aqueous solutions considerably underestimate the maximum actinide concentrations.

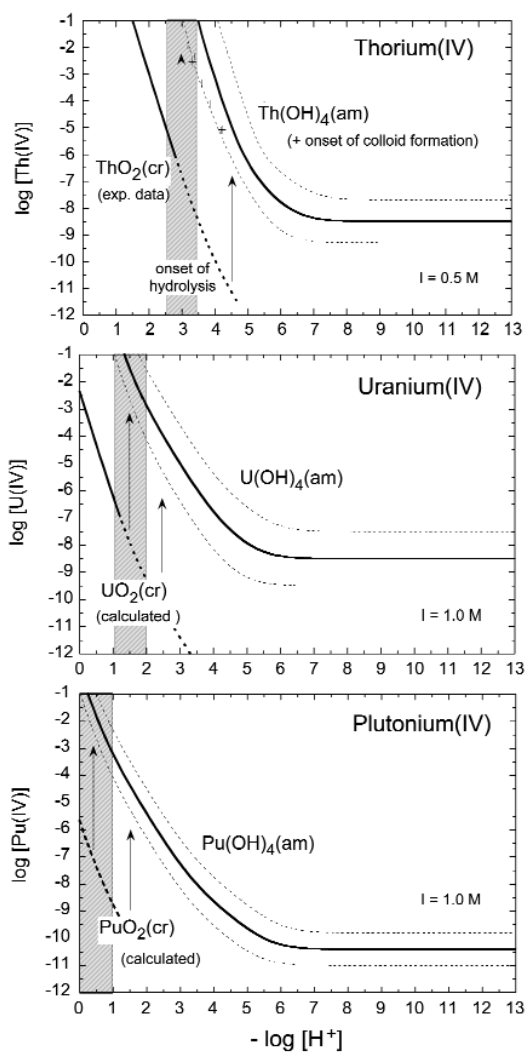


Fig. 8 Solubility of crystalline and amorphous An(IV) oxides/hydroxides. The arrows indicate that, above the onset of hydrolysis (hatched area), the irreversible dissolution of $AnO_2(cr)$ leads to solubility data expected for the amorphous solids.

REFERENCES

1. I. Grenthe, J. Fuger, R. J. M. Konings, R. J. Lemire, A. B. Muller, C. Nguyen-Trung, H. Wanner (OECD, NEA). *Chemical Thermodynamics of Uranium*, Elsevier, North-Holland (1992).
2. R. J. Silva, G. Bidoglio, M. H. Rand, P. Robouch, H. Wanner, I. Puigdomenech (OECD, NEA). *Chemical Thermodynamics of Americium*, Elsevier, North-Holland (1995).
3. R. J. Lemire, J. Fuger, H. Nitsche, P. Potter, M. H. Rand, J. Rydberg, K. Spahiu, J. C. Sullivan, W. J. Ullman, P. Vitorge, H. Wanner (OECD, NEA). *Chemical Thermodynamics of Neptunium and Plutonium*, Elsevier, North-Holland (2001).
4. R. Guillaumont, Th. Fanghänel, J. Fuger, I. Grenthe, V. Neck, D. A. Palmer, M. H. Rand (OECD, NEA). Update of the *Chemical Thermodynamics of Uranium, Neptunium, Plutonium, Americium, and Technetium*. In preparation.
5. G. R. Choppin. *Radiochim. Acta* **32**, 43 (1983).
6. G. R. Choppin and E. N. Rizkalla. In *Handbook on the Physics and Chemistry of Rare Earths*, K. A. Gschneidner, Jr. and L. Eyring (Eds.), **18**, pp. 559–590, North Holland, Amsterdam (1994).
7. Th. Fanghänel and J. I. Kim. *J. Alloys Comp.* **271–273**, 728 (1998).
8. I. Pashalidis, K. R. Czerwinski, Th. Fanghänel, J. I. Kim. *Radiochim. Acta* **76**, 55 (1997).
9. V. Neck and J. I. Kim. *Radiochim. Acta* **89**, 1 (2001).
10. C. F. Baes, Jr. and R. E. Mesmer. *The Hydrolysis of Cations*, Wiley, New York (1976).
11. I. Grenthe and I. Puigdomenech. *Modelling in Aquatic Chemistry*, OECD, NEA, Paris (1997).
12. D. Shannon. *Acta Cryst. A* **32**, 751 (1976).
13. V. Neck, Th. Fanghänel, J. I. Kim. Report FZKA 6110, Karlsruhe (1998).
14. W. Runde and J. I. Kim. Report RCM 01094, Technische Universität München (1994).
15. W. Runde, M. P. Neu, D. L. Clark. *Geochim. Cosmochim. Acta* **60**, 2065 (1996).
16. A. Cassol, L. Magon, G. Tomat, R. Portanova. *Inorg. Chem.* **11**, 515 (1972).
17. V. Neck and J. I. Kim. *Radiochim. Acta* **88**, 815 (2000).
18. D. Rai, J. L. Swanson, J. L. Ryan. *Radiochim. Acta* **42**, 35 (1987).
19. J. Fuger and F. L. Oetting. *The Chemical Thermodynamics of Actinide Elements and Compounds, Part 2. The Actinide Aqueous Ions*, IAEA, Vienna, Austria (1976).
20. Ch. Lierse, W. Treiber, J. I. Kim. *Radiochim. Acta* **38**, 27 (1985).
21. V. Neck, J. I. Kim, B. Kanellakopulos. *Radiochim. Acta* **56**, 25 (1992).
22. K. E. Roberts, H. B. Silber, P. Torretto, T. Prussin, K. Becraft, D. E. Hobart, C. F. Novak. *Radiochim. Acta* **74**, 27 (1996).
23. L. Merli and J. Fuger. *Radiochim. Acta* **66/67**, 109 (1994).
24. P. Pan and A. B. Campbell. *Radiochim. Acta* **81**, 73 (1998).
25. D. W. Efurud, W. Runde, J. C. Banar, D. R. Janecky, J. P. Kaszuba, P. D. Palmer, F. R. Roensch, C. D. Tait. *Environ. Sci. Technol.* **32**, 3893 (1998).
26. U. Kramer-Schnabel, H. Bischoff, R. H. Xi, G. Marx. *Radiochim. Acta* **56**, 183 (1992).
27. M. C. A. Sandino and J. Bruno. *Geochim. Cosmochim. Acta* **56**, 4135 (1992).
28. G. Meinrath and T. Kimura. *Inorg. Chim. Acta* **204**, 79 (1993).
29. M. E. Torrero, I. Casas, J. de Pablo, M. C. A. Sandino, B. Grambow. *Radiochim. Acta* **66/67**, 29 (1994).
30. G. Meinrath, Y. Kato, T. Kimura, Z. Yoshida. *Radiochim. Acta* **75**, 159 (1996).
31. Y. Kato, T. Kimura, Z. Yoshida, N. Nitani. *Radiochim. Acta* **74**, 21 (1996).
32. T. Yamamura, A. Kitamura, A. Fukui, S. Nishikawa, T. Yamamoto, H. Moriyama. *Radiochim. Acta* **83**, 139 (1998).
33. M. Altmaier, V. Neck, R. Müller, A. Bauer, Th. Fanghänel. Unpublished results.
34. R. J. Silva. Report LBL-15055, Lawrence Berkeley Laboratory, Berkeley (1982).
35. S. Stadler and J. I. Kim. *Radiochim. Acta* **44/45**, 39 (1988).
36. D. Rai, R. G. Strickert, D. A. Moore, J. L. Ryan. *Radiochim. Acta* **33**, 201 (1983).

37. N. M. Edelstein, J. Bucher, R. J. Silva, H. Nitsche. Report ONWI-399, LBL-15055, Lawrence Berkeley Laboratory, Berkeley (1983).
38. H. Nitsche and N. M. Edelstein. *Radiochim. Acta* **39**, 23 (1985).
39. B. I. Nabivanets and L. N. Kudritskaya. *Ukr. Khim. Zh.* **30**, 891 (1964).
40. H. C. Moon. *Bull. Korean Chem. Soc.* **10**, 270 (1989).
41. J. L. Ryan and D. Rai. *Inorg. Chem.* **26**, 4140 (1987).
42. A. R. Felmy, D. Rai, M. J. Mason. *Radiochim. Acta* **55**, 177 (1991).
43. D. Rai, A. R. Felmy, S. M. Sterner, D. A. Moore, M. J. Mason, C. F. Novak. *Radiochim. Acta* **79**, 239 (1997).
44. D. Rai, D. A. Moore, C. S. Oakes, M. Yui. *Radiochim. Acta* **88**, 297 (2000).
45. E. Östhols, J. Bruno, I. Grenthe. *Geochim. Cosmochim. Acta* **58**, 613 (1994).
46. V. Neck, R. Müller, M. Bouby, M. Altmaier, J. Rothe, M. A. Denecke, J. I. Kim. Proc. Int. Conf. Migration '01, Bregenz, Austria, Oct. 2001, *Radiochim. Acta*. In press.
47. C. Bitea, R. Müller, V. Neck, C. Walther, J. I. Kim. Proc. E-MRS Spring Meeting, Symp. Colloid 2000, Strasbourg, France, June 2002, *Colloids Surf., A*. In press.
48. P. W. Schindler. *Adv. Chem. Ser.* **67**, 196 (1967).
49. T. Bundschuh, R. Knopp, R. Müller, J. I. Kim, V. Neck, Th. Fanghänel. *Radiochim. Acta* **88**, 625 (2000).
50. V. Neck, M. Altmaier, R. Müller, A. Bauer, Th. Fanghänel, J. I. Kim. *Radiochim. Acta*. Accepted for publication.
51. D. J. Dzimitrowicz, P. J. Wiseman, D. Cherns. *J. Coll. Interf. Sci.* **103**, 170 (1985).
52. S. Hubert, K. Barthelet, B. Fourest, G. Lagarde, N. Dacheux, N. Baglan. *J. Nucl. Mat.* **297**, 206 (2001).
53. B. Fourest, T. Vincent, G. Lagarde, S. Hubert, P. Baudoin. *J. Nucl. Mat.* **282**, 180 (2000).